Measurement of $\mathcal{B}(J/\psi \to \eta' e^+ e^-)$ and search for a dark photon

M. Ablikim,[1] M. N. Achasov,[9,d] S. Ahmed,[14] M. Albrecht,[4] M. Alekseev,[55a,55c] A. Amoroso,[55a,55c] F. F. An,[1] Q. An,[52,42] J. Z. Bai,[1] Y. Bai,[41] O. Bakina,[26] R. Baldini Ferroli,[22a] Y. Ban,[34] K. Begzsuren,[24] D. W. Bennett,[21] J. V. Bennett,[5] N. Berger,[25] M. Bertani,[22a] D. Bettoni,[23a] F. Bianchi,[55a,55c] E. Boger,[26,b] I. Boyko,[26] R. A. Briere,[5] H. Cai,[57] X. Cai,[1,42] O. Cakir,[45a] A. Calcaterra,[22a] G. F. Cao,[1,46] S. A. Cetin,[45b] J. Chai,[55c] J. F. Chang,[1,42] G. Chelkov,[26,b,c] G. Chen,[1] H. S. Chen,[1,46] J. C. Chen,[1] M. L. Chen,[1,42] P. L. Chen,[53] S. J. Chen,[32] X. R. Chen,[29] Y. B. Chen,[1,42] X. K. Chu,[34] G. Cibinetto,[23a] F. Cossio,[55c] H. L. Dai,[1,42] J. P. Dai,[37,h] A. Dbeyssi,[14] D. Dedovich,[26] Z. Y. Deng,[1] A. Denig,[25] I. Denysenko,[26] M. Destefanis,[55a,55c] F. De Mori,[55a,55c] Y. Ding,[30] C. Dong,[33] J. Dong,[1,42] L. Y. Dong,[1,46] M. Y. Dong,[1,42,46] Z. L. Dou,[32] S. X. Du,[60] P. F. Duan,[1] J. Fang,[1,42] S. S. Fang,[1,46] Y. Fang,[1] R. Farinelli,[23a,23b] L. Fava,[55b,55c] S. Fegan,[25] F. Feldbauer,[4] G. Felici,[22a] C. Q. Feng,[52,42] E. Fioravanti,[23a] M. Fritsch,[4] C. D. Fu,[1] Q. Gao,[1] X. L. Gao,[52,42] Y. Gao,[44] Y. G. Gao,[6] Z. Gao,[52,42] B. Garillon,[25] I. Garzia,[23a] A. Gilman,[49] K. Goetzen,[10] L. Gong,[33] W. X. Gong,[1,42] W. Gradl,[25] M. Greco,[55a,55c] M. H. Gu,[1,42] Y. T. Gu,[12] A. Q. Guo,[1] R. P. Guo,[1,46] Y. P. Guo,[25] A. Guskov,[26] Z. Haddadi,[28] S. Han,[57] X. Q. Hao,[15] F. A. Harris,[47] K. L. He,[1,46] X. Q. He,[51] F. H. Heinsius,[4] T. Held,[4] Y. K. Heng,[1,42,46] T. Holtmann,[4] Z. L. Hou,[1] H. M. Hu,[1,46] J. F. Hu,[37,h] T. Hu,[1,42,46] Y. Hu,[1] G. S. Huang,[52,42] J. S. Huang,[15] X. T. Huang,[36] X. Z. Huang,[32] Z. L. Huang,[30] T. Hussain,[54] W. Ikegami Andersson,[56] M. Irshad,[52,42] Q. Ji,[1] Q. P. Ji,[15] X. B. Ji,[1,46] X. L. Ji,[1,42] X. S. Jiang,[1,42,46] X. Y. Jiang,[33] J. B. Jiao,[36] Z. Jiao,[17] D. P. Jin,[1,42,46] S. Jin,[1,46] Y. Jin,[48] T. Johansson,[56] A. Julin,[49] N. Kalantar-Nayestanaki,[28] X. S. Kang,[33] M. Kavatsyuk,[28] B. C. Ke,[1] T. Khan,[52,42] A. Khoukaz,[50] P. Kiese,[25] R. Kliemt,[10] L. Koch,[27] O. B. Kolcu,[45b,f] B. Kopf,[4] M. Kornicer,[47] M. Kuemmel,[4] M. Kuessner,[4] A. Kupsc,[56] M. Kurth,[1] W. Kühn,[27] J. S. Lange,[27] M. Lara,[21] P. Larin,[14] L. Lavezzi,[55c] H. Leithoff,[25] C. Li,[56] Cheng Li,[52,42] D. M. Li,[60] F. Li,[1,42] F. Y. Li,[34,*] G. Li,[1] H. B. Li,[1,46] H. J. Li,[1,46] J. C. Li,[1] J. W. Li,[40] Jin Li,[35] K. J. Li,[43] Kang Li,[13] Ke Li,[1] Lei Li,[3] P. L. Li,[52,42] P. R. Li,[46,7] Q. Y. Li,[36] W. D. Li,[1,46] W. G. Li,[1] X. L. Li,[36] X. N. Li,[1,42] X. Q. Li,[33] Z. B. Li,[43] H. Liang,[52,42] Y. F. Liang,[39] Y. T. Liang,[27] G. R. Liao,[11] L. Z. Liao,[1,46] J. Libby,[20] C. X. Lin,[43] D. X. Lin,[14] B. Liu,[37,h] B. J. Liu,[1] C. X. Liu,[1] D. Liu,[52,42] D. Y. Liu,[37,h] F. H. Liu,[38] Fang Liu,[1] Feng Liu,[6] H. B. Liu,[12] H. L. Liu,[41] H. M. Liu,[1,46] Huanhuan Liu,[1] Huihui Liu,[16] J. B. Liu,[52,42] J. Y. Liu,[1,46] K. Liu,[44] K. Y. Liu,[30] Ke Liu,[6] L. D. Liu,[34] Q. Liu,[46] S. B. Liu,[52,42] X. Liu,[29] Y. B. Liu,[33] Z. A. Liu,[1,42,46] Zhiqing Liu,[25] Y. F. Long,[34] X. C. Lou,[1,42,46] H. J. Lu,[17] J. G. Lu,[1,42] Y. Lu,[1] Y. P. Lu,[1,42] C. L. Luo,[31] M. X. Luo,[59] X. L. Luo,[1,42] S. Lusso,[55c] X. R. Lyu,[46] F. C. Ma,[30] H. L. Ma,[1] L. L. Ma,[36] M. M. Ma,[1,46] Q. M. Ma,[1] T. Ma,[1] X. N. Ma,[33] X. Y. Ma,[1,42] Y. M. Ma,[36] F. E. Maas,[14] M. Maggiora,[55a,55c] Q. A. Malik,[54] A. Mangoni,[22b] Y. J. Mao,[34] Z. P. Mao,[1] S. Marcello,[55a,55c] Z. X. Meng,[48] J. G. Messchendorp,[28] G. Mezzadri,[23b] J. Min,[1,42] R. E. Mitchell,[21] X. H. Mo,[1,42,46] Y. J. Mo,[6] C. Morales Morales,[14] N. Yu. Muchnoi,[9,d] H. Muramatsu,[49] A. Mustafa,[4] Y. Nefedov,[26] F. Nerling,[10] I. B. Nikolaev,[9,d] Z. Ning,[1,42] S. Nisar,[8] S. L. Niu,[1,42] X. Y. Niu,[1,46] S. L. Olsen,[35,j] Q. Ouyang,[1,42,46] S. Pacetti,[22b] Y. Pan,[52,42] M. Papenbrock,[56] P. Patteri,[22a] M. Pelizaeus,[4] J. Pellegrino,[55a,55c] H. P. Peng,[52,42] Z. Y. Peng,[12] K. Peters,[10,g] J. Pettersson,[56] J. L. Ping,[31] R. G. Ping,[1,46] A. Pitka,[4] R. Poling,[49] V. Prasad,[52,42] H. R. Qi,[2] M. Qi,[32] T. Y. Qi,[2] S. Qian,[1,42] C. F. Qiao,[46] N. Qin,[57] X. S. Qin,[4] Z. H. Qin,[1,42] J. F. Qiu,[1] K. H. Rashid,[54,i] C. F. Redmer,[25] M. Richter,[4] M. Ripka,[25] M. Rolo,[55c] G. Rong,[1,46] Ch. Rosner,[14] A. Sarantsev,[26,e] M. Savrié,[23b] C. Schnier,[4] K. Schoenning,[56] W. Shan,[18] X. Y. Shan,[52,42] M. Shao,[52,42] C. P. Shen,[2] P. X. Shen,[33] X. Y. Shen,[1,46] H. Y. Sheng,[1] X. Shi,[1,42] J. J. Song,[36] W. M. Song,[36] X. Y. Song,[1] S. Sosio,[55a,55c] C. Sowa,[4] S. Spataro,[55a,55c] G. X. Sun,[1] J. F. Sun,[15] L. Sun,[57] S. S. Sun,[1,46] X. H. Sun,[1] Y. J. Sun,[52,42] Y. K. Sun,[52,42] Y. Z. Sun,[1] Z. J. Sun,[1,42] Z. T. Sun,[21] Y. T. Tan,[52,42] C. J. Tang,[39] G. Y. Tang,[1] X. Tang,[1] I. Tapan,[45c] M. Tiemens,[28] B. Tsednee,[24] I. Uman,[45d] G. S. Varner,[47] B. Wang,[1] B. L. Wang,[46] D. Wang,[34] D. Y. Wang,[34] Dan Wang,[46] K. Wang,[1,42] L. L. Wang,[1] L. S. Wang,[1] M. Wang,[36] Meng Wang,[1,46] M. Z. Wang,[34] P. Wang,[1] P. L. Wang,[1] W. P. Wang,[52,42] X. F. Wang,[44] Y. Wang,[52,42] Y. F. Wang,[1,42,46] Y. Q. Wang,[25] Z. Wang,[1,42] Z. G. Wang,[1,42] Z. Y. Wang,[1] Zongyuan Wang,[1,46] T. Weber,[4] D. H. Wei,[11] P. Weidenkaff,[25] S. P. Wen,[1] U. Wiedner,[4] M. Wolke,[56] L. H. Wu,[1] L. J. Wu,[1,46] Z. Wu,[1,42] L. Xia,[52,42] Y. Xia,[19] D. Xiao,[1] Y. J. Xiao,[1,46] Z. J. Xiao,[31] Y. G. Xie,[1,42] Y. H. Xie,[6] X. A. Xiong,[1,46] Q. L. Xiu,[1,42] G. F. Xu,[1] J. J. Xu,[1,46] L. Xu,[1] Q. J. Xu,[13] Q. N. Xu,[46] X. P. Xu,[40] F. Yan,[53] L. Yan,[55a,55c] W. B. Yan,[52,42] W. C. Yan,[2] Y. H. Yan,[19] H. J. Yang,[37,h] H. X. Yang,[1] L. Yang,[57] Y. H. Yang,[32] Y. X. Yang,[11] Yifan Yang,[1,46] M. Ye,[1,42] M. H. Ye,[7] J. H. Yin,[1] Z. Y. You,[43] B. X. Yu,[1,42,46] C. X. Yu,[33] J. S. Yu,[29] C. Z. Yuan,[1,46] Y. Yuan,[1] A. Yuncu,[45b,a] A. A. Zafar,[54] Y. Zeng,[19] Z. Zeng,[52,42] B. X. Zhang,[1] B. Y. Zhang,[1,42] C. C. Zhang,[1] D. H. Zhang,[1] H. H. Zhang,[43] H. Y. Zhang,[1,42] J. Zhang,[1,46] J. L. Zhang,[58] J. Q. Zhang,[4] J. W. Zhang,[1,42,46] J. Y. Zhang,[1] J. Z. Zhang,[1,46] K. Zhang,[1,46] L. Zhang,[44] T. J. Zhang,[37,h] X. Y. Zhang,[36] Y. Zhang,[52,42] Y. H. Zhang,[1,42] Y. T. Zhang,[52,42] Yang Zhang,[1] Yao Zhang,[1] Yu Zhang,[46] Z. H. Zhang,[6] Z. P. Zhang,[52] Z. Y. Zhang,[57] G. Zhao,[1] J. W. Zhao,[1,42] J. Y. Zhao,[1,46] J. Z. Zhao,[1,42] Lei Zhao,[52,42] Ling Zhao,[1] M. G. Zhao,[33] Q. Zhao,[1] S. J. Zhao,[60] T. C. Zhao,[1] Y. B. Zhao,[1,42] Z. G. Zhao,[52,42] A. Zhemchugov,[26,b] B. Zheng,[53] J. P. Zheng,[1,42] Y. H. Zheng,[46] B. Zhong,[31] L. Zhou,[1,42] Q. Zhou,[1,46] X. Zhou,[57] X. K. Zhou,[52,42] X. R. Zhou,[52,42] X. Y. Zhou,[1] A. N. Zhu,[1,46]

J. Zhu,[33] J. Zhu,[43] K. Zhu,[1] K. J. Zhu,[1,42,46] S. Zhu,[1] S. H. Zhu,[51] X. L. Zhu,[44] Y. C. Zhu,[52,42] Y. S. Zhu,[1,46] Z. A. Zhu,[1,46] J. Zhuang,[1,42] B. S. Zou,[1] and J. H. Zou[1]

(BESIII Collaboration)

[1]*Institute of High Energy Physics, Beijing 100049, People's Republic of China*
[2]*Beihang University, Beijing 100191, People's Republic of China*
[3]*Beijing Institute of Petrochemical Technology, Beijing 102617, People's Republic of China*
[4]*Bochum Ruhr-University, D-44780 Bochum, Germany*
[5]*Carnegie Mellon University, Pittsburgh, Pennsylvania 15213, USA*
[6]*Central China Normal University, Wuhan 430079, People's Republic of China*
[7]*China Center of Advanced Science and Technology, Beijing 100190, People's Republic of China*
[8]*COMSATS Institute of Information Technology, Lahore, Defence Road, Off Raiwind Road, 54000 Lahore, Pakistan*
[9]*G.I. Budker Institute of Nuclear Physics SB RAS (BINP), Novosibirsk 630090, Russia*
[10]*GSI Helmholtzcentre for Heavy Ion Research GmbH, D-64291 Darmstadt, Germany*
[11]*Guangxi Normal University, Guilin 541004, People's Republic of China*
[12]*Guangxi University, Nanning 530004, People's Republic of China*
[13]*Hangzhou Normal University, Hangzhou 310036, People's Republic of China*
[14]*Helmholtz Institute Mainz, Johann-Joachim-Becher-Weg 45, D-55099 Mainz, Germany*
[15]*Henan Normal University, Xinxiang 453007, People's Republic of China*
[16]*Henan University of Science and Technology, Luoyang 471003, People's Republic of China*
[17]*Huangshan College, Huangshan 245000, People's Republic of China*
[18]*Hunan Normal University, Changsha 410081, People's Republic of China*
[19]*Hunan University, Changsha 410082, People's Republic of China*
[20]*Indian Institute of Technology Madras, Chennai 600036, India*
[21]*Indiana University, Bloomington, Indiana 47405, USA*
[22a]*INFN Laboratori Nazionali di Frascati, I-00044, Frascati, Italy*
[22b]*INFN and University of Perugia, I-06100, Perugia, Italy*
[23a]*INFN Sezione di Ferrara, I-44122, Ferrara, Italy*
[23b]*University of Ferrara, I-44122, Ferrara, Italy*
[24]*Institute of Physics and Technology, Peace Avenue 54B, Ulaanbaatar 13330, Mongolia*
[25]*Johannes Gutenberg University of Mainz, Johann-Joachim-Becher-Weg 45, D-55099 Mainz, Germany*
[26]*Joint Institute for Nuclear Research, 141980 Dubna, Moscow Region, Russia*
[27]*Justus-Liebig-Universitaet Giessen, II. Physikalisches Institut, Heinrich-Buff-Ring 16, D-35392 Giessen, Germany*
[28]*KVI-CART, University of Groningen, NL-9747 AA Groningen, The Netherlands*
[29]*Lanzhou University, Lanzhou 730000, People's Republic of China*
[30]*Liaoning University, Shenyang 110036, People's Republic of China*
[31]*Nanjing Normal University, Nanjing 210023, People's Republic of China*
[32]*Nanjing University, Nanjing 210093, People's Republic of China*
[33]*Nankai University, Tianjin 300071, People's Republic of China*
[34]*Peking University, Beijing 100871, People's Republic of China*
[35]*Seoul National University, Seoul, 151-747 Korea*
[36]*Shandong University, Jinan 250100, People's Republic of China*
[37]*Shanghai Jiao Tong University, Shanghai 200240, People's Republic of China*
[38]*Shanxi University, Taiyuan 030006, People's Republic of China*
[39]*Sichuan University, Chengdu 610064, People's Republic of China*
[40]*Soochow University, Suzhou 215006, People's Republic of China*
[41]*Southeast University, Nanjing 211100, People's Republic of China*
[42]*State Key Laboratory of Particle Detection and Electronics, Beijing 100049, Hefei 230026, People's Republic of China*
[43]*Sun Yat-Sen University, Guangzhou 510275, People's Republic of China*
[44]*Tsinghua University, Beijing 100084, People's Republic of China*
[45a]*Ankara University, 06100 Tandogan, Ankara, Turkey*
[45b]*Istanbul Bilgi University, 34060 Eyup, Istanbul, Turkey*
[45c]*Uludag University, 16059 Bursa, Turkey*
[45d]*Near East University, Nicosia, North Cyprus, Mersin 10, Turkey*
[46]*University of Chinese Academy of Sciences, Beijing 100049, People's Republic of China*
[47]*University of Hawaii, Honolulu, Hawaii 96822, USA*

[48]University of Jinan, Jinan 250022, People's Republic of China
[49]University of Minnesota, Minneapolis, Minnesota 55455, USA
[50]University of Muenster, Wilhelm-Klemm-Str. 9, 48149 Muenster, Germany
[51]University of Science and Technology Liaoning, Anshan 114051, People's Republic of China
[52]University of Science and Technology of China, Hefei 230026, People's Republic of China
[53]University of South China, Hengyang 421001, People's Republic of China
[54]University of the Punjab, Lahore-54590, Pakistan
[55a]University of Turin, I-10125, Turin, Italy
[55b]University of Eastern Piedmont, I-15121, Alessandria, Italy
[55c]INFN, I-10125, Turin, Italy
[56]Uppsala University, Box 516, SE-75120 Uppsala, Sweden
[57]Wuhan University, Wuhan 430072, People's Republic of China
[58]Xinyang Normal University, Xinyang 464000, People's Republic of China
[59]Zhejiang University, Hangzhou 310027, People's Republic of China
[60]Zhengzhou University, Zhengzhou 450001, People's Republic of China

(Received 3 September 2018; published 28 January 2019)

Using a data sample of $(1310.6 \pm 7.0) \times 10^6$ J/ψ decay events collected with the BESIII detector at BEPCII, we study the electromagnetic Dalitz decay $J/\psi \to \eta' e^+ e^-$ with two dominant η' decay modes, $\eta' \to \gamma\pi^+\pi^-$ and $\eta' \to \pi^+\pi^-\eta$. The branching fraction is determined to be $\mathcal{B}(J/\psi \to \eta' e^+ e^-) = (6.59 \pm 0.07 \pm 0.17) \times 10^{-5}$, which improves in precision by a factor of 2 over the previous BESIII measurement. A search for the dark photon (γ') is performed via $J/\psi \to \eta'\gamma', \gamma' \to e^+e^-$. Excluding the ω and ϕ mass regions, no significant signal is observed in the mass range from 0.1 to 2.1 GeV/c^2. We set upper limits at the 90% confidence level on $\mathcal{B}(J/\psi \to \eta'\gamma') \times \mathcal{B}(\gamma' \to e^+e^-)$, $\mathcal{B}(J/\psi \to \eta'\gamma')$ and the mixing strength as a function of dark photon mass. This is among the first searches for dark photons in charmonium decays.

DOI: 10.1103/PhysRevD.99.012013

I. INTRODUCTION

The electromagnetic (EM) Dalitz decay of a vector meson (V) to a pseudoscalar meson (P) and a pair of leptons ($l = e$, μ), $V \to Pl^+l^-$, provides important information on the interaction at the V-P transition vertex [1], where the lepton pair in the final state originates from a virtual photon. Such Dalitz processes have been widely studied with light unflavored meson decays, such as $\phi \to \pi^0 e^+ e^-$ [2], $\omega \to \pi^0 e^+ e^-$ [3,4], $\omega \to \pi^0 \mu^+ \mu^-$ [5] and $\phi \to \eta e^+ e^-$ [6,7]. BESIII observed the decays $J/\psi \to P e^+ e^-$ [8] for the first time using $(225.3 \pm 2.8) \times 10^6$ J/ψ events. The branching fraction (BF) of $J/\psi \to \eta' e^+ e^-$ was measured to be $(5.81 \pm 0.16 \pm 0.31) \times 10^{-5}$. It agrees with the theoretical prediction $(5.66 \pm 0.16) \times 10^{-5}$ [9] within the uncertainty.

Except for gravitational effects, we still know very little about the constituents and interactions of dark matter. Many models beyond the Standard Model (SM) of particle physics have proposed the existence of a dark sector, which is being searched for with efforts from different types of experiments [10–20]. The simple realizations of these models usually consist of an extra U(1) gauge group, with a corresponding massive vector boson force carrier, called a dark photon (γ'), which is neutral under the SM gauge symmetries, but couples to the SM photon via kinetic mixing [21] and decays into SM particles. Such models provide a natural scenario for dark matter interactions. A dark photon with a mass in the MeV/c^2 to GeV/c^2 range

*Corresponding author.
lify@pku.edu.cn
[a]Also at Bogazici University, 34342 Istanbul, Turkey.
[b]Also at the Moscow Institute of Physics and Technology, Moscow 141700, Russia.
[c]Also at the Functional Electronics Laboratory, Tomsk State University, Tomsk, 634050, Russia.
[d]Also at the Novosibirsk State University, Novosibirsk, 630090, Russia.
[e]Also at the NRC "Kurchatov Institute," PNPI, 188300, Gatchina, Russia.
[f]Also at Istanbul Arel University, 34295 Istanbul, Turkey.
[g]Also at Goethe University Frankfurt, 60323 Frankfurt am Main, Germany.
[h]Also at Key Laboratory for Particle Physics, Astrophysics and Cosmology, Ministry of Education; Shanghai Key Laboratory for Particle Physics and Cosmology; Institute of Nuclear and Particle Physics, Shanghai 200240, People's Republic of China.
[i]Government College Women University, Sialkot - 51310, Punjab, Pakistan.
[j]Present address: Center for Underground Physics, Institute for Basic Science, Daejeon 34126, Korea.

can also be accommodated by observational astroparticle anomalies [22]. Low-energy electron-positron colliders offer an ideal environment to test these low-mass dark sector models [23,24], and meson decays provide an important constraint on the mixing strength ε between the dark photon and SM photon [25,26]. The authors of Ref. [9] have estimated the achievable limits on the mixing strength in the processes $J/\psi \to P\gamma'(\gamma' \to l^+l^-)$ using the huge BESIII J/ψ data sample. The search in J/ψ decays could uniquely probe the coupling of the dark photon with the charm quark.

In this paper, we report on the updated BF measurement of $J/\psi \to \eta' e^+e^-$ and a search for a dark photon through $J/\psi \to \eta'\gamma', \gamma' \to e^+e^-$, with 405 pb^{-1} e^+e^- collision data containing $(1310.6 \pm 7.0) \times 10^6$ J/ψ events [27] collected by BESIII. Together with the study of $J/\psi \to \eta e^+e^-$ [28] with the same data set, it is the first time that the dark photon is searched for through the charmonium decays.

II. APPARATUS AND MONTE CARLO SIMULATION

BEPCII is a double ring e^+e^- collider running at the center-of-mass (c.m.) energy $\sqrt{s}$ from 2.0 to 4.6 GeV with a peaking luminosity of 1×10^{33} cm^{-2} s^{-1}. The BESIII detector [29], with a geometrical acceptance of 93% of the 4π stereo angle, operates in a magnetic field of 1.0 T (0.9 T in 2012) provided by a superconducting solenoid. It is composed of a helium-based main drift chamber (MDC) to measure the momentum and ionization energy loss (dE/dx) of charged particles, a plastic scintillator time-of-flight (TOF) system for particle identification (PID) information, a CsI(Tl) electromagnetic calorimeter (EMC) to measure photon and electron energies and a multilayer resistive plate chamber muon detection system to identify muons.

Monte Carlo (MC) simulations are used to optimize the event selection, investigate background and determine the detection efficiency. The GEANT4-based [30] simulation includes the description of the geometry and material of the BESIII detector, the detector response, and digitization models and also tracks the detector running conditions and performance. An inclusive MC sample containing 1.225×10^9 J/ψ events is used to study potential backgrounds. The production of the J/ψ meson is simulated by the MC event generator KKMC [31]. The known decay modes of the J/ψ are generated by EVTGEN [32] with BFs set at the world average values from the particle data group (PDG) [33], while the remaining unknown decays are generated by LUNDCHARM [34]. The analysis is performed in the framework of the BESIII offline software system which takes care of the detector calibration and event reconstruction.

The decay $J/\psi \to \eta' e^+e^-$ is simulated according to the Lorentz-invariant amplitude, taking into account the J/ψ polarization state in the e^+e^- annihilation system. The J/ψ to η' transition form factor is assumed to be a single-pole form $|F(q^2)| = 1/(1 - q^2/\Lambda^2)$, where q^2 is the four-momentum transfer squared and Λ is the effective pole mass, with a value of $\Lambda = 3.686$ GeV/c^2. Then the subsequent decay mode of $\eta' \to \gamma\pi^+\pi^-$ is simulated with the ρ-ω interference and box anomaly effects [35,36]. The decays of $\eta' \to \pi^+\pi^-\eta$ and $\eta \to \gamma\gamma$ are generated with a phase space model. The decays of $J/\psi \to \eta' V$ (V represents ρ, ω, ϕ) and $J/\psi \to \eta'\gamma'$ are generated by a P-wave decay model, and the decay $\gamma' \to e^+e^-$ is modeled as a vector meson decaying to a lepton pair [32].

III. DATA ANALYSIS

In this work, the signal is reconstructed with a pair of an electron and positron, in addition to an η' meson, which is reconstructed with two decay modes of $\eta' \to \gamma\pi^+\pi^-$ and $\eta' \to \pi^+\pi^-\eta(\gamma\gamma)$. The final states of the corresponding J/ψ decays are $\gamma\pi^+\pi^-e^+e^-$ and $\gamma\gamma\pi^+\pi^-e^+e^-$, respectively. They are denoted as mode I and mode II throughout this paper.

Charged tracks in the BESIII detector are reconstructed from hits in the MDC. We select good charged tracks passing within ± 10 cm from the interaction point (IP) in the beam direction and within 1 cm in the plane perpendicular to the beam. The polar angle of the track is required to satisfy $|\cos\theta| < 0.93$. Four candidate charged tracks are required, and their net charge must be equal to zero. The combined information of the energy loss dE/dx from the MDC and the time of flight from the TOF is used to calculate the PID confidence levels (C.L.) for the e, π and K hypotheses. Both the electron and positron selections require the electron hypothesis to have the highest PID C.L. among the three hypotheses, and the other two charged tracks are treated as $\pi^+\pi^-$ candidates without any PID requirement. The four charged tracks $\pi^+\pi^-e^+e^-$ must pass a common vertex constrained fit to ensure that they originate from the interaction point.

Electromagnetic showers are reconstructed from clusters of energy deposits in the EMC. The shower energy of photon candidates in the EMC must be greater than 25 MeV in the barrel region ($|\cos\theta| < 0.80$) or 50 MeV in the end-cap region ($0.86 < |\cos\theta| < 0.92$). Showers located between the barrel and end-cap regions are excluded due to worse reconstruction. Showers are required to be separated from the extrapolated positions of any charged track by more than 10°. Cluster-timing requirements are used to suppress electronic noise and unrelated energy deposits. We require at least one (two) candidate photon(s) for mode I (II). The η meson is reconstructed with $\gamma\gamma$ state, with the $\gamma\gamma$ invariant mass $M(\gamma\gamma)$ of candidates required to be within $[0.48, 0.60]$ GeV/c^2.

A four-constraint (4C) energy-momentum conservation kinematic fit is performed to the signal hypothesis. For events with extra photon candidates, the combination of final state particles with the minimum chi-square ($\chi^2_{\rm 4C}$)

is selected, and the χ^2_{4C} is required to be less than 100. The χ^2_{4C} requirement removes more than 12% and 30% of background events for mode I and II, respectively, and results in a signal efficiency loss of about 7% for both modes.

A. Measurement of $\mathcal{B}(J/\psi \to \eta' e^+ e^-)$

The major background that can peak in η' mass distribution is from the radiative decay $J/\psi \to \gamma\eta'$ followed by a γ conversion process, where γ converts into an e^+e^- pair when it interacts with material in front of the MDC. The distance from the reconstructed vertex of the e^+e^- pair to the IP in the x-y projection, δ_{xy}, is used to identify γ conversion [37]. Here $\delta_{xy} = \sqrt{R_x^2 + R_y^2}$, and R_x and R_y are the coordinates of the reconstructed vertex in the x and y directions. The scatter plot of R_y versus R_x of the $J/\psi \to \gamma\eta'(\eta' \to \gamma\pi^+\pi^-)$ MC sample, and the δ_{xy} distributions of data and various MC samples are shown in Fig. 1. The two peaks above 2 cm in the δ_{xy} distribution match the positions of the beam pipe and inner wall of the MDC. Only events with $\delta_{xy} < 2$ cm are retained. The normalized number of the remaining γ conversion events is estimated according to the corresponding BFs from the PDG [33], as 202.2 ± 7.3 (70.6 ± 2.5) in mode I (II).

In addition to the γ conversion events, there are some other minor backgrounds that can also peak in η' mass distribution. The background from $J/\psi \to V\eta'$, $V = \rho$, ω, ϕ decays is studied with high statistics MC samples. The peaking background from the process $J/\psi \to \eta'\pi^+\pi^-$ is estimated with a MC sample generated according to the amplitude as reported in Ref. [38]. The numbers of these background events ($N^{\rm bkg}$), normalized according to the world-averaged BFs [33], are summarized in Table I. Potential peaking background from the two-photon process $e^+e^- \to e^+e^-\eta'$ is found to be negligible, as studied with 2.93 fb^{-1} of data at c.m. energy of 3.773 GeV [39,40].

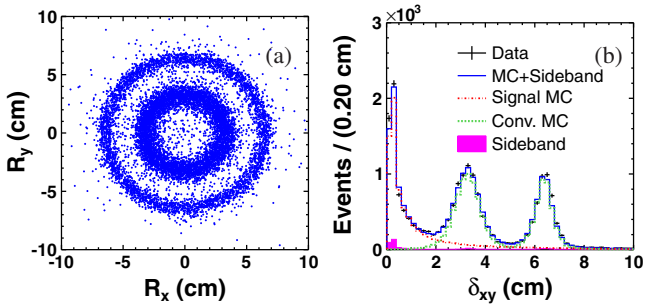

FIG. 1. Electron-positron pair vertex distributions. (a) The two-dimensional scatter plot of R_y versus R_x from $J/\psi \to \gamma\eta'(\eta' \to \gamma\pi^+\pi^-)$ MC simulated events. (b) Distribution of δ_{xy}. The black crosses are data, the blue solid line is the total contribution from the MC and η' sideband, the green dotted-dashed line is signal MC, the dashed line is $J/\psi \to \gamma\eta'(\eta' \to \gamma\pi^+\pi^-)$ MC and the shaded area is the η' sideband. The quantities are described in the text.

TABLE I. Number of nonconversion peaking background events, as estimated with high statistics MC. The uncertainties include those of all intermediate resonance decay BFs [33]. "…" indicates cases of no event survival. The first group lists contributions from $J/\psi \to \phi\eta'(\phi \to e^+e^-)$, as fixed in the fitting, and $J/\psi \to \rho\eta'(\rho \to \pi^+\pi^-)$, which is included coherently in $J/\psi \to \eta'\pi^+\pi^-$. The second group shows minor contribution sources, which are not accounted for in the fitting, but needs to be subtracted from the fitted signal yield.

	$N^{\rm bkg}$ (mode I)	$N^{\rm bkg}$ (mode II)
$J/\psi \to \phi\eta'(\phi \to e^+e^-)$	17.1 ± 1.9	6.4 ± 0.7
$J/\psi \to \rho\eta'(\rho \to \pi^+\pi^-)$	2.8 ± 0.2	0.8 ± 0.1
$J/\psi \to \omega\eta'(\omega \to e^+e^-)$	1.6 ± 0.2	0.6 ± 0.1
$J/\psi \to \rho\eta'(\rho \to e^+e^-)$	0.48 ± 0.05	0.18 ± 0.02
$J/\psi \to \phi\eta'(\phi \to K^+K^-)$	…	…
$J/\psi \to \eta'\pi^+\pi^-$	3.8 ± 0.2	1.8 ± 0.1
Contribution to subtract	5.9 ± 0.3	2.5 ± 0.2

Mode II has no obvious nonpeaking contamination of the η' invariant mass distribution, and the background containing an η is determined to be negligible from a MC study. There are two kinds of nonpeaking background for mode I. One is $J/\psi \to \pi^+\pi^-\eta/\pi^0$ with $\eta/\pi^0 \to \gamma e^+e^-$, which has the same final state $\gamma\pi^+\pi^-e^+e^-$ as the signal process. To reject the background with a π^0 intermediate state, candidates with the γe^+e^- invariant mass $M(\gamma e^+e^-)$ in the π^0 mass window $[0.10, 0.16]$ GeV/c^2 are removed. The other is from J/ψ decays with multiple pions in the final state, where a pion pair is misidentified as an electron-positron pair. Both backgrounds produce a smooth shape on the $\gamma\pi^+\pi^-$ invariant mass $M(\gamma\pi^+\pi^-)$ distribution around the η' mass.

The distributions of $\gamma\pi^+\pi^-$ invariant mass $M(\gamma\pi^+\pi^-)$ and $\gamma\gamma\pi^+\pi^-$ invariant mass $M(\gamma\gamma\pi^+\pi^-)$ of surviving candidate events after all the above selection criteria, within the region $[0.87, 1.03]$ GeV/c^2, are shown in Fig. 2.

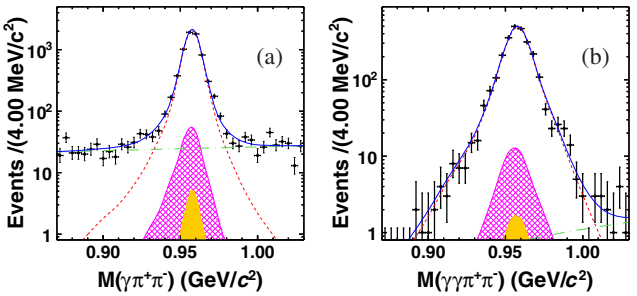

FIG. 2. The invariant mass spectra of η' candidate events (a) $M(\gamma\pi^+\pi^-)$ and (b) $M(\gamma\gamma\pi^+\pi^-)$. Black crosses are data, the blue solid line is the total fitting projection, the red dashed line is signal, the green dotted-dashed line is nonpeaking background, the pink cross-hatched area is γ conversion $J/\psi \to \gamma\eta'$ and the yellow solid area is $J/\psi \to \eta'\phi$, $\phi \to e^+e^-$.

Unbinned maximum likelihood (ML) fits are performed on the $M(\gamma\pi^+\pi^-)$ and $M(\gamma\gamma\pi^+\pi^-)$ distributions to determine the signal yields. In the fits, the signal probability density function (PDF) is described by a signal MC simulated shape convolved with a Gaussian function, which takes into account the resolution difference between data and MC simulation. The major peaking backgrounds from γ conversion $J/\psi \to \gamma\eta'$ and $J/\psi \to \phi\eta'(\phi \to e^+e^-)$ are described with MC shapes, and their magnitudes are fixed to the expected values. The number of minor peaking background events as shown in Table I is directly subtracted from the fitted η' yields. The nonpeaking backgrounds in mode I and II are described with second- and first-order Chebyshev polynomial functions, respectively. The fit results are shown in Fig. 2, with signal yields of 6442.8 ± 87.1 and 2497.9 ± 51.3 for mode I and II, respectively. The goodness of fit is demonstrated by χ^2 over the number of degrees of freedom (ndf), with values $\chi^2/\text{ndf} = 74.8/35$ and $34.3/17$ for mode I and II, respectively. The BF of $J/\psi \to \eta' e^+e^-$ is determined by

$$\mathcal{B}(J/\psi \to \eta' e^+e^-) = \frac{N_{\rm sig}}{N_{J/\psi} \cdot \mathcal{B}_{\eta' \to \rm F} \cdot \mathcal{E} \cdot \delta^2}, \qquad (1)$$

where $N_{\rm sig}$ is the number of signal events, $N_{J/\psi}$ is the number of J/ψ events, $\mathcal{B}_{\eta' \to \rm F}$ is the intermediate BF of the η' decay, $(28.9 \pm 0.5)\%$ for $\mathcal{B}(\eta' \to \gamma\pi^+\pi^-)$ in mode I and $(16.9 \pm 0.3)\%$ for $\mathcal{B}(\eta' \to \eta\pi^+\pi^-) \times \mathcal{B}(\eta \to \gamma\gamma)$ in mode II [33], $\mathcal{E}$ is the detection efficiency $(25.01 \pm 0.06)\%$ for mode I and $(16.82 \pm 0.06)\%$ for mode II and $\delta = 1.012$ is the tracking efficiency correction factor per electron/positron as described in Sec. IV. Using Eq. (1) and taking into account the systematic uncertainties discussed in Sec. IV, $\mathcal{B}(J/\psi \to \eta' e^+e^-)$ values for mode I and mode II are calculated to be $(6.63 \pm 0.09 \pm 0.21) \times 10^{-5}$ and $(6.54 \pm 0.13 \pm 0.26) \times 10^{-5}$, respectively, where the first uncertainties are statistical and the second are systematic. The results from the two η' decay modes are consistent with each other within the statistical and uncorrelated systematic uncertainties. With the weighted least squares method taking into account the correlated and uncorrelated uncertainties [41], the weighted average BF from the two decay modes is $\mathcal{B}(J/\psi \to \eta' e^+e^-) = (6.59 \pm 0.07 \pm 0.17) \times 10^{-5}$. This result is consistent with the previous BESIII measurement [8], and the precision is improved by a factor of 2, from 6% to 3%. The measured value is higher than the theoretical prediction of Ref. [9] from the single-pole form factor and will provide further input to improve theoretical models.

B. Search for the dark photon through $J/\psi \to \eta' e^+e^-$

The dark photon is searched for by looking for a narrow resonance peaking on a smooth electron-positron invariant mass $[M(e^+e^-)]$ spectrum at the position of the dark photon mass ($m_{\gamma'}$). Candidate events with the $\eta' e^+e^-$ final state are selected with the same selection criteria as described in Sec. III A but without the γ conversion veto criteria. Since γ conversion events distribute mainly in the low $M(e^+e^-)$ region below 70 MeV/c^2, only candidate events with $M(e^+e^-) > 70\,\text{MeV}/c^2$ are retained. The mass ranges $[0.74, 0.84]$ GeV/c^2 and $[1.00, 1.04]$ GeV/c^2, corresponding to the regions of the ω and ϕ mesons, are excluded in the dark photon search, since the search sensitivity of $\gamma' \to e^+e^-$ would degrade significantly due to the complicated SM background and the suppressed BF of $\gamma' \to e^+e^-$ [23,26,42]. The invariant mass of the η' candidates is required to be within $[0.93, 0.98]$ GeV/c^2 and the selected events are mainly from the EM Dalitz decay $J/\psi \to \eta' e^+e^-$.

The signal PDF and detection efficiency are determined with a series of signal MC samples. They are generated according to the decay chain $J/\psi \to \eta'\gamma'$, $\gamma' \to e^+e^-$, with different $m_{\gamma'}$ values, ranging from 0.1 to 2.0 GeV/c^2 with a step of 0.1 GeV/c^2. The dark photon width, suppressed by a factor of ε^2 and expected to be far below the experimental resolution, is set to zero in the MC generation. The dark photon signal PDF is parametrized by the sum of two Crystal Ball (CB) functions with a common mean value, where the parameters are determined by fitting the signal MC samples. The resolution, which is evaluated by weighting the widths of two CBs according to their ratio, grows from 2 to 8 MeV/c^2 as $m_{\gamma'}$ increases. The detection efficiency, shown in Fig. 3, ranges from 35% to 41% and from 22% to 27% depending on $m_{\gamma'}$ in mode I and II, respectively. The efficiency and signal PDF parameters are interpolated between the mass points by a fit with a polynomial function. The background PDF is the sum of a second-order polynomial function and an exponential function: $f(m_{e^+e^-}) = c_2 \cdot m^2_{e^+e^-} + c_1 \cdot m_{e^+e^-} + c_0 + e^{c_3 \cdot m_{e^+e^-}}$. The parameters c_0, c_1, c_2, and c_3 are determined from a background-only ML fit of data as shown in Figs. 4(a) and 4(b).

To determine the possible dark photon signal yield, a series of ML fits are performed in the range

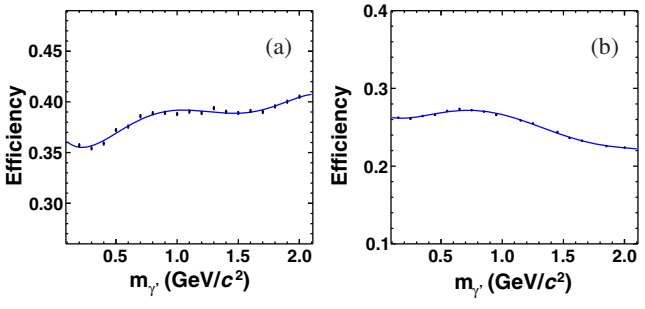

FIG. 3. The total detection efficiency of the entire decay chain for different $m_{\gamma'}$ of (a) mode I and (b) mode II. The blue curves show the fit with polynomial functions.

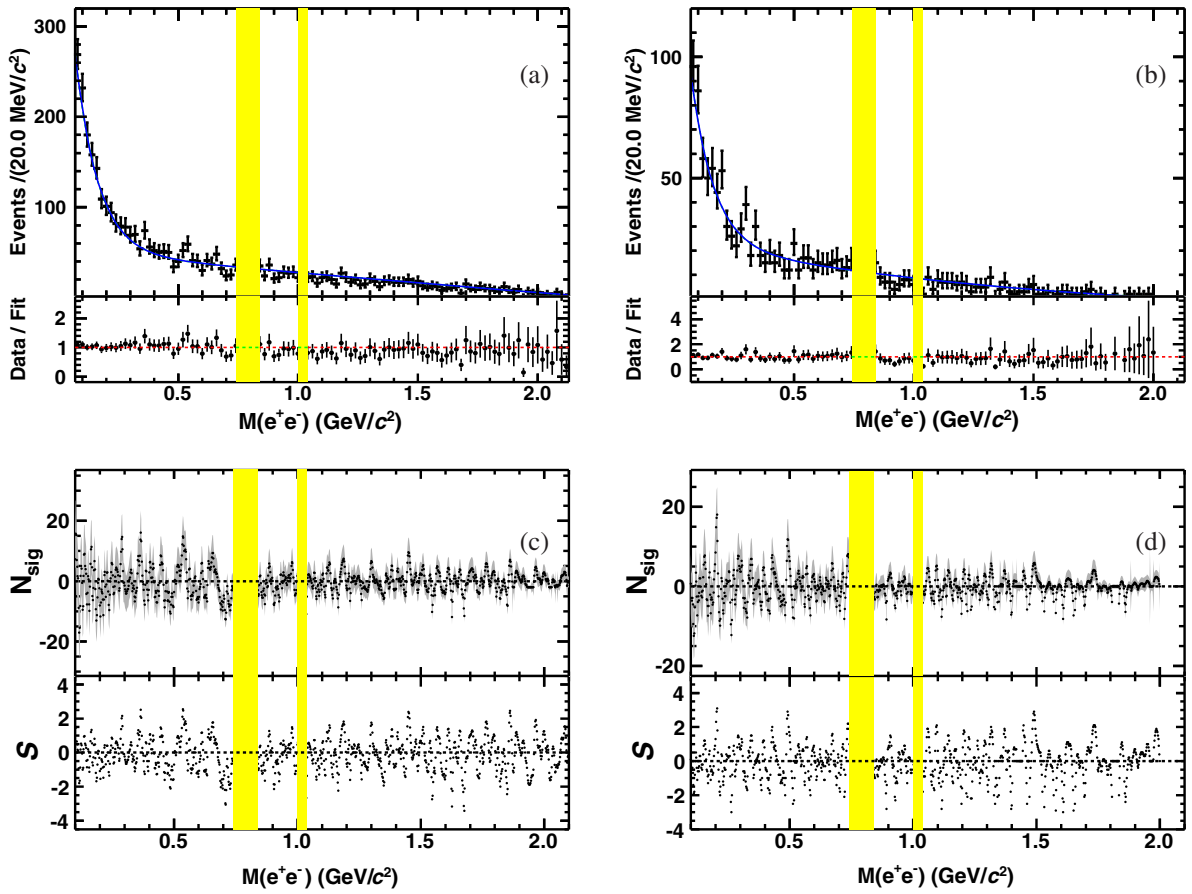

FIG. 4. The upper plots in (a) and (b) show the electron-positron pair invariant mass distributions for mode I and mode II, respectively, where the crosses are data and the solid lines are the background-only fitting results. The lower plots in (a) and (b) show the ratio of data over fitting result for each bin. The shaded bands are the corresponding excluded ω and ϕ regions. The plots in (c) and (d) are the number of signal events ($N_{\rm sig}$) and the significances (S) from the fit for mode I and mode II, respectively.

$0.07 < m_{\gamma'} < 2.13\ \mathrm{GeV}/c^2$ with uniform mass steps of $2\ \mathrm{MeV}/c^2$. In each fit, a composite PDF model of the corresponding signal shape and the common background description is used, with the parameters of the signal and background fixed while their yields are free to float. In order to avoid fit failure due to the limited statistics in the high $M(e^+e^-)$ region in mode II, a lower bound on the signal yield is imposed by requiring the total PDF of signal plus background to remain non-negative.

For each $M(e^+e^-)$ point, the local significance of the signal is determined by $\mathcal{S} = \mathrm{sign}(N_{\rm sig})\sqrt{-2\ln(\mathcal{L}_0/\mathcal{L}_{\rm max})}$, where $\mathcal{L}_0$ ($\mathcal{L}_{\rm max}$) is the likelihood value without (with) the signal hypothesis included in the fit. The results of $N_{\rm sig}$ and the corresponding significance are shown in Figs. 4(c) and 4(d), respectively. The maximum local significance is from mode II, with 3.1σ at $0.204\ \mathrm{GeV}/c^2$. The corresponding global significance is less than 1σ, evaluated by using a large number of pseudoexperiments [43]. In conclusion, no significant dark photon signal is observed within the searched range.

IV. SYSTEMATIC UNCERTAINTIES

Most of the systematic uncertainties from the event selection are the same for the BF measurement and the dark photon search. The correlations between the two η' reconstruction modes are taken into account when evaluating the uncertainties for the BF measurement. The uncertainties for the efficiencies of MDC tracking, photon detection, PID, the number of J/ψ decay events, and the γ conversion veto are considered as correlated sources. Those for an additional photon in $\eta' \to \pi^+\pi^-\eta(\gamma\gamma)$, the 4C kinematic fit, η reconstruction, the form factor, signal shape, fit range, background shape and magnitude and η' BFs are considered as the independent sources. The systematic uncertainties are discussed below and summarized in Table II.

Some of the uncertainties are estimated in a similar way as described in Ref. [8]. The uncertainty is 0.6% per electron due to PID, determined by comparing the efficiency difference between data and MC simulation for a control sample of radiative Bhabha $e^+e^- \to \gamma e^+e^-$

TABLE II. Sources of systematic uncertainties for the BF measurement and multiplicative terms for the dark photon search (in %). The correlated sources between $\eta' \to \gamma\pi^+\pi^-$ and $\eta' \to \pi^+\pi^-\eta(\gamma\gamma)$ modes are marked with an asterisk.

	BF measurement		Search for dark photon	
Sources	$\eta' \to \gamma\pi^+\pi^-$	$\eta' \to \pi^+\pi^-\eta(\gamma\gamma)$	$\eta' \to \gamma\pi^+\pi^-$	$\eta' \to \pi^+\pi^-\eta(\gamma\gamma)$
MDC tracking *	1.6	2.4	1.6	2.4
PID *	1.2	1.2	1.2	1.2
Photon detection *	0.6	1.2	0.6	1.2
4C kinematic fit	0.5	0.5	0.5	0.5
Veto of γ conversion *	1.0	1.0	…	…
η reconstruction	…	1.0	…	1.0
Form factor	0.4	0.2	…	…
Signal shape	0.4	0.2	…	…
Fit range and background shape	0.6	1.3	…	…
Fixed peaking background	0.3	0.3	…	…
Number of J/ψ events *	0.5	0.5	0.5	0.5
η' BFs	1.7	1.7	1.7	1.7
$\mathcal{B}(\gamma' \to e^+e^-)$*	…	…	$-^{a}/(0\text{–}14)^{b}$	$-^{a}/(0\text{–}14)^{b}$
Total	3.1	4.0	$2.8^{a}/(2.8\text{–}14.3)^{b}$	$3.6^{a}/(3.6\text{–}14.5)^{b}$

[a]Uncertainties associated with the upper limit on $\mathcal{B}(J/\psi \to \eta'\gamma') \times \mathcal{B}(\gamma' \to e^+e^-)$.
[b]Uncertainties associated with the upper limit on $\mathcal{B}(J/\psi \to \eta'\gamma')$.

(including $J/\psi \to \gamma e^+e^-$) events collected at the J/ψ energy. With the same control sample, the electron tracking efficiency from MC is corrected in a two-dimensional distribution of the transverse momentum versus polar angle of the lepton tracks by different interpolation algorithms event by event. The difference between data and MC after correction shows consistent values of 0.5% per track, which is taken as the electron tracking uncertainty, and the overall efficiency correction factor per electron/positron track is calculated to be $\delta = 1.012$. The charged pion tracking efficiency is studied with the control sample of $J/\psi \to \pi^+\pi^- p\bar{p}$ events. The differences between data and MC are tabulated in bins of transverse momentum and polar angle. After reweighting according to the signal kinematics, the tracking uncertainties for charged pions are determined to be 0.3% per pion track in mode I and 0.7% in mode II, reflecting the different pion transverse momentum distributions of the two modes. Tracking uncertainties are treated as fully correlated and thus added linearly.

The photon detection efficiency is studied with a control sample of $J/\psi \to \pi^+\pi^-\pi^0$, $\pi^0 \to \gamma\gamma$ events. The data/MC difference is 0.5% (1.5%) for a photon in the EMC barrel (end-cap) region. The average difference, 0.6% per photon, is taken as systematic uncertainty.

The uncertainty associated with the 4C kinematic fit is estimated with a high purity control sample of $J/\psi \to \pi^+\pi^-\pi^0$, $\pi^0 \to \gamma e^+e^-$ events. The efficiency difference between data and MC simulation is 0.5%, which is taken as the systematic uncertainty. This control sample is also used to estimate the uncertainty due to the γ conversion veto criterion $\delta_{xy} < 2$ cm. The difference in efficiency between data and MC simulation is 1% and is taken as the uncertainty.

The signal efficiency may also be biased due to the η reconstruction via its $\gamma\gamma$ decay. The systematic uncertainty for it is determined to be 1.0% from a study of the control sample of $J/\psi \to p\bar{p}\eta$ [44] events.

The uncertainty of the transition form factor used in the MC generation is estimated with the alternative signal MC samples generated with the parameters $\Lambda = 3.0$ or 4.0 GeV/c^2, and the largest efficiency difference 0.4% (0.2%) with respect to the nominal one is taken as the uncertainty for mode I (II).

The uncertainty on the efficiency due to the choice of the signal parametrization is 0.4% (0.2%) for mode I (II), evaluated by comparing the signal yields with and without the Gaussian function convolution in the fit. We select alternative fit ranges and a higher order Chebyshev polynomial function for nonpeaking background shapes to estimate the related uncertainty. The largest difference of the signal yield with respect to the nominal one, 0.6% (1.3%), is taken as the uncertainty for mode I (II). The uncertainty due to fixing the peaking-background yield is 0.3% for both modes, evaluated by adjusting the number of peaking background events by one standard deviation of the total peaking background yield.

The uncertainty of the number of J/ψ events is determined to be 0.5% [27] and those of the η' BFs are taken as 1.7% for both modes [33].

For the dark photon search, the systematic uncertainties are divided into additive and multiplicative terms. The additive systematic uncertainties arise from the fit bias and the signal and background PDFs. The multiplicative uncertainties come from the number of J/ψ events, η' BFs and detection efficiencies, which have been discussed

in the BF measurement. To incorporate these uncertainties, we take the additive systematic uncertainty into consideration by performing the same fit procedure with different combinations of the nominal and alternative fit ranges, signal shapes and background shapes. The maximum number of signal events among the different fit scenarios is adopted to calculate the upper limit of the signal yield $N_{\rm sig}$. This procedure is performed for mode I and mode II separately. The multiplicative systematic uncertainties in the search for a dark photon are listed in Table II. Most of them come from differences in the selection efficiency between data and MC simulation. When deriving $\mathcal{B}(J/\psi \to \eta'\gamma')$ from the product BF, an additional systematic uncertainty originates from the theoretical BF of $\mathcal{B}(\gamma' \to e^+e^-)$, which is 0–14% depending on $m_{\gamma'}$ according to Ref. [23] and mainly comes from the R value measurement.

V. DARK PHOTON SEARCH RESULT

We compute the upper limit on the BFs $\mathcal{B}(J/\psi \to \eta'\gamma') \times \mathcal{B}(\gamma' \to e^+e^-)$ and $\mathcal{B}(J/\psi \to \eta'\gamma')$ at the 90% C.L. using a Bayesian method [33]. The expected number of signal events observed in the ith mode is calculated with $N^i_{\rm sig} = N_{J/\psi} \cdot \mathcal{B}^i_{\eta' \to \rm F} \cdot \mathcal{B}(J/\psi \to \gamma'\eta') \cdot \mathcal{B}(\gamma' \to e^+e^-) \cdot \mathcal{E}^i \cdot \delta^2$, where $N_{J/\psi}$ is the number of J/ψ events, $\mathcal{B}^i_{\eta' \to \rm F}$ is the BF of η' decay to final state F, $\mathcal{B}(J/\psi \to \gamma'\eta')$ and $\mathcal{B}(\gamma' \to e^+e^-)$ are the BFs' signal MC simulation, and $\delta = 1.012$ is the electron tracking efficiency correction factor. The likelihood value ($\mathcal{L}$), as a function of product BF $\mathcal{B}(J/\psi \to \eta'\gamma') \times \mathcal{B}(\gamma' \to e^+e^-)$, is calculated as a product of $\mathcal{L}$ from mode I and mode II with the method described in Ref. [45]. The systematic uncertainties, which have been discussed in Sec. IV, are separately incorporated into the likelihood distribution as correlated and uncorrelated terms. The upper limit $\mathcal{B}^{\rm UP}$ on the product BF at the 90% C.L. is determined from the integral $\int_0^{\mathcal{B}^{\rm UP}} \mathcal{L} d\mathcal{B} / \int_0^{\infty} \mathcal{L} d\mathcal{B} = 90\%$. The values of $\mathcal{B}^{\rm UP}$ are plotted as a function of $m_{\gamma'}$ in Fig. 5(a). We also obtain the likelihood value as a function of $\mathcal{B}(J/\psi \to \eta'\gamma')$ by taking into account the BF $\mathcal{B}(\gamma' \to e^+e^-)$ and its corresponding uncertainty [23], and we compute the upper limit on the $\mathcal{B}(J/\psi \to \eta'\gamma')$ at the 90% C.L., as shown in Fig. 5(b). The upper limit at the 90% C.L. on the BF $\mathcal{B}(J/\psi \to \eta'\gamma') \times \mathcal{B}(\gamma' \to e^+e^-)$ ranges from 1.8×10^{-8} to 2.0×10^{-7} and that on $\mathcal{B}(J/\psi \to \eta'\gamma')$ ranges from 5.7×10^{-8} to 7.4×10^{-7}.

The mixing strength ε coupling γ' and SM photon is determined from the ratio of the BF $\mathcal{B}(J/\psi \to \eta'\gamma')$ and that of the radiative process $\mathcal{B}(J/\psi \to \eta'\gamma)$ as [26]

$$\frac{\mathcal{B}(J/\psi \to \eta'\gamma')}{\mathcal{B}(J/\psi \to \eta'\gamma)} = \varepsilon^2 |F(m^2_{\gamma'})|^2 \frac{\lambda^{3/2}(m^2_{J/\psi}, m^2_{\eta'}, m^2_{\gamma'})}{\lambda^{3/2}(m^2_{J/\psi}, m^2_{\eta'}, 0)},$$

where $\lambda(m_1^2, m_2^2, m_3^2) = (1 + \frac{m_3^2}{m_1^2 - m_2^2})^2 - \frac{4m_1^2 m_3^2}{(m_1^2 - m_2^2)^2}$; m_i is the mass of a specific particle i; and $|F(m^2_{\gamma'})|^2$ is the J/ψ to η' transition form factor as described in Sec. II, evaluated at $q^2 = m^2_{\gamma'}$. The BF $\mathcal{B}(J/\psi \to \eta'\gamma)$ is taken from the PDG [33] value. The corresponding exclusion limit on the mixing strength ε, which is shown in Fig. 5(c), ranges from 3.4×10^{-3} to 2.6×10^{-2} depending on $m_{\gamma'}$.

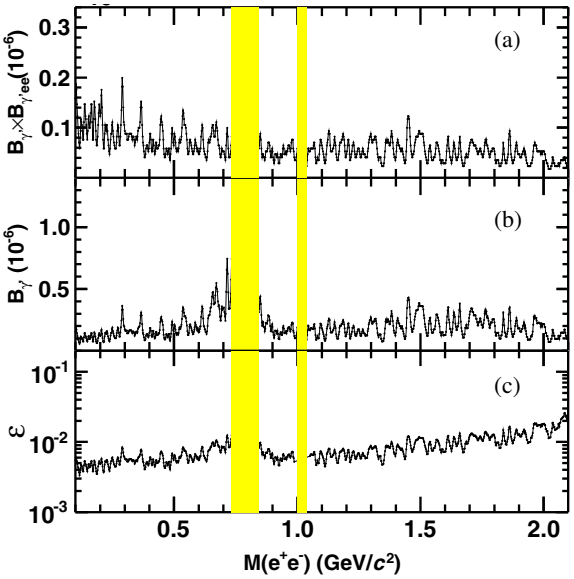

FIG. 5. Upper limits at the 90% C.L. for the BFs (a) $\mathcal{B}_{\gamma'} \times \mathcal{B}_{\gamma' \rm ee}$ and (b) $\mathcal{B}_{\gamma'}$, where $\mathcal{B}_{\gamma'}$ and $\mathcal{B}_{\gamma' \rm ee}$ are $\mathcal{B}(J/\psi \to \eta'\gamma')$ and $\mathcal{B}(\gamma' \to e^+e^-)$, respectively. (c) The exclusion limit at the 90% C.L. on the kinematic mixing strength ε.

VI. SUMMARY

With a data sample of $(1310.6 \pm 7.0) \times 10^6$ J/ψ events collected by the BESIII detector, we measure the BF of the EM Dalitz decay $J/\psi \to \eta' e^+ e^-$ with two dominant η' decay modes. The combined result of $\mathcal{B}(J/\psi \to \eta' e^+ e^-)$ is determined to be $(6.59 \pm 0.07 \pm 0.17) \times 10^{-5}$. This result is compatible with the previous BESIII measurement [8] and the precision is greatly improved from 6% to 3%.

We also search for a dark photon via the decay chain $J/\psi \to \eta'\gamma', \gamma' \to e^+e^-$ with the same two η' decay modes. No significant signal of γ' is observed, and we set upper limits for the product BF $\mathcal{B}(J/\psi \to \eta'\gamma') \times \mathcal{B}(\gamma' \to e^+e^-)$ and the BF $\mathcal{B}(J/\psi \to \eta'\gamma')$ at the 90% C.L., which range from 1.8×10^{-8} to 2.0×10^{-7} and 5.7×10^{-8} to 7.4×10^{-7}, respectively. The exclusion limit on the mixing strength ε between the SM photon and dark photon varies in a range from 3.4×10^{-3} to 2.6×10^{-2} depending on $m_{\gamma'}$. This is among the first searches for the dark photon in the charmonium decays.

ACKNOWLEDGMENTS

The BESIII Collaboration thanks the staff of BEPCII and the IHEP computing center for their strong support. This

work is supported in part by National Key Basic Research Program of China under Contract No. 2015CB856700; National Natural Science Foundation of China (NSFC) under Contracts No. 11235011, No. 11335008, No. 11425524, No. 11625523, and No. 11635010; the Chinese Academy of Sciences (CAS) Large-Scale Scientific Facility Program; the CAS Center for Excellence in Particle Physics (CCEPP); Joint Large-Scale Scientific Facility Funds of the NSFC and CAS under Contracts No. U1232105, No. U1332201, No. U1532257, and No. U1532258; CAS Key Research Program of Frontier Sciences under Contracts No. QYZDJ-SSW-SLH003 and No. QYZDJ-SSW-SLH040; 100 Talents Program of CAS; National 1000 Talents Program of China; INPAC and Shanghai Key Laboratory for Particle Physics and Cosmology; German Research Foundation DFG under Contracts No. Collaborative Research Center CRC 1044 and No. FOR 2359; Instituto Nazionale di Fisica Nucleare, Italy; Koninklijke Nederlandse Akademie van Wetenschappen (KNAW) under Contract No. 530-4CDP03; Ministry of Development of Turkey under Contract No. DPT2006K-120470; National Science and Technology fund; The Swedish Research Council; U.S. Department of Energy under Contracts No. DE-FG02-05ER41374, No. DE-SC-0010118, No. DE-SC-0010504, and No. DE-SC-0012069; University of Groningen (RuG) and the Helmholtzzentrum fuer Schwerionenforschung GmbH (GSI), Darmstadt; WCU Program of National Research Foundation of Korea under Contract No. R32-2008-000-10155-0.

[1] L. G. Landsberg, Phys. Rep. **128**, 301 (1985).
[2] A. Anastasi *et al.* (KLOE-2 Collaboration), Phys. Lett. B **757**, 362 (2016).
[3] R. R. Akhmetshin *et al.* (CMD-2 Collaboration), Phys. Lett. B **613**, 29 (2005).
[4] P. Adlarson *et al.* (A2 Collaboration), Phys. Rev. C **95**, 035208 (2017).
[5] R. Arnaldi *et al.* (NA60 Collaboration), Phys. Lett. B **677**, 260 (2009).
[6] M. N. Achasov *et al.* (SND Collaboration), Phys. Lett. B **504**, 275 (2001).
[7] D. Babusci *et al.* (KLOE-2 Collaboration), Phys. Lett. B **742**, 1 (2015).
[8] M. Ablikim *et al.* (BESIII Collaboration), Phys. Rev. D **89**, 092008 (2014).
[9] J. Fu, H. B. Li, X. Qin, and M. Z. Yang, Mod. Phys. Lett. A **27**, 1250223 (2012).
[10] B. Aubert *et al.* (*BABAR* Collaboration), Phys. Rev. Lett. **103**, 081803 (2009).
[11] H. Merkel *et al.* (A1 Collaboration), Phys. Rev. Lett. **106**, 251802 (2011).
[12] S. Abrahamyan *et al.* (APEX Collaboration), Phys. Rev. Lett. **107**, 191804 (2011).
[13] F. Archilli *et al.* (KLOE-2 Collaboration), Phys. Lett. B **706**, 251 (2012).
[14] H. Merkel *et al.* (A1 Collaboration), Phys. Rev. Lett. **112**, 221802 (2014).
[15] J. P. Lees *et al.* (*BABAR* Collaboration), Phys. Rev. Lett. **113**, 201801 (2014).
[16] J. R. Batley *et al.* (NA48/2 Collaboration), Phys. Lett. B **746**, 178 (2015).
[17] A. Anastasi *et al.*, Phys. Lett. B **750**, 633 (2015).
[18] A. Anastasi *et al.* (KLOE-2 Collaboration), Phys. Lett. B **757**, 356 (2016).
[19] M. Ablikim *et al.* (BESIII Collaboration), Phys. Lett. B **774**, 252 (2017).
[20] R. Aaij *et al.* (LHCb Collaboration), Phys. Rev. Lett. **120**, 061801 (2018).
[21] B. Holdom, Phys. Lett. **166B**, 196 (1986).
[22] N. Arkani-Hamed, D. P. Finkbeiner, T. R. Slatyer, and N. Weiner, Phys. Rev. D **79**, 015014 (2009).
[23] B. Batell, M. Pospelov, and A. Ritz, Phys. Rev. D **79**, 115008 (2009).
[24] R. Essig, P. Schuster, and N. Toro, Phys. Rev. D **80**, 015003 (2009).
[25] P. Fayet, Phys. Rev. D **75**, 115017 (2007).
[26] M. Reece and L.-T. Wang, J. High Energy Phys. 07 (2009) 051.
[27] M. Ablikim *et al.* (BESIII Collaboration), Chin. Phys. C **41**, 013001 (2017).
[28] M. Ablikim *et al.* (BESIII Collaboration), Phys. Rev. D **99**, 012006 (2019).
[29] M. Ablikim *et al.* (BESIII Collaboration), Nucl. Instrum. Methods Phys. Res., Sect. A **614**, 345 (2010).
[30] S. Agostinelli *et al.* (GEANT4 Collaboration), Nucl. Instrum. Methods Phys. Res., Sect. A **506**, 250 (2003).
[31] S. Jadach, B. F. L. Ward, and Z. Was, Comput. Phys. Commun. **130**, 260 (2000); Phys. Rev. D **63**, 113009 (2001).
[32] D. J. Lange, Nucl. Instrum. Methods Phys. Res., Sect. A **462**, 152 (2001); R. G. Ping, Chin. Phys. C **32**, 599 (2008).
[33] M. Tanabashi *et al.* (Particle Data Group), Phys. Rev. D **98**, 030001 (2018).
[34] J. C. Chen, G. S. Huang, X. R. Qi, D. H. Zhang, and Y. S. Zhu, Phys. Rev. D **62**, 034003 (2000).
[35] M. Ablikim *et al.* (BESIII Collaboration), Phys. Rev. D **87**, 092011 (2013).
[36] M. Ablikim *et al.* (BESIII Collaboration), Phys. Rev. Lett. **120**, 242003 (2018).
[37] Z. R. Xu and K. L. He, Chin. Phys. C **36**, 742 (2012).
[38] M. Ablikim *et al.* (BESIII Collaboration), Phys. Rev. D **96**, 112012 (2017).

[39] M. Ablikim *et al.* (BESIII Collaboration), Chin. Phys. C **37**, 123001 (2013).
[40] M. Ablikim *et al.* (BESIII Collaboration), Phys. Lett. B **753**, 629 (2016).
[41] G. D'Agostini, Nucl. Instrum. Methods Phys. Res., Sect. A **346**, 306 (1994).
[42] H. Li and T. Luo, Phys. Lett. B **686**, 249 (2010).
[43] M. Ablikim *et al.* (BESIII Collaboration), Phys. Rev. D **93**, 052005 (2016).
[44] M. Ablikim *et al.* (BESIII Collaboration), Phys. Rev. D **81**, 052005 (2010).
[45] K. Stenson, arXiv:physics/0605236.